HHS Public Access

Author manuscript

Acta Biomater. Author manuscript; available in PMC 2018 August 01.

Published in final edited form as:

Acta Biomater. 2017 August ; 58: 479–491. doi:10.1016/j.actbio.2017.05.026.

Nanodiamond-based injectable hydrogel for sustained growth factor release: Preparation, characterization and *in vitro* analysis

Settimio Pacelli[a], **Francisca Acosta**[a], **Aparna R. Chakravarti**[a], **Saheli G. Samanta**[b], **Jonathan Whitlow**[a], **Saman Modaresi**[a], **Rafeeq P.H. Ahmed**[c], **Johnson Rajasingh**[b], and **Arghya Paul**[a,*]

[a]BioIntel Research Laboratory, Department of Chemical and Petroleum Engineering, School of Engineering, University of Kansas, Lawrence, KS, United States

[b]Department of Internal Medicine, Cardiovascular Research Institute, University of Kansas Medical Center, Kansas City, KS, United States

[c]Department of Pathology, University of Cincinnati, 231-Albert Sabin Way, Cincinnati 45267, United States

Abstract

Nanodiamonds (NDs) represent an emerging class of carbon nanomaterials that possess favorable physical and chemical properties to be used as multifunctional carriers for a variety of bioactive molecules. Here we report the synthesis and characterization of a new injectable ND-based nanocomposite hydrogel which facilitates a controlled release of therapeutic molecules for regenerative applications. In particular, we have formulated a thermosensitive hydrogel using gelatin, chitosan and NDs that provides a sustained release of exogenous human vascular endothelial growth factor (VEGF) for wound healing applications. Addition of NDs improved the mechanical properties of the injectable hydrogels without affecting its thermosensitive gelation properties. Biocompatibility of the generated hydrogel was verified by *in vitro* assessment of apoptotic gene expressions and anti-inflammatory interleukin productions. NDs were complexed with VEGF and the inclusion of this complex in the hydrogel network enabled the sustained release of the angiogenic growth factor. These results suggest for the first time that NDs can be used to formulate a biocompatible, thermosensitive and multifunctional hydrogel platform that can function both as a filling agent to modulate hydrogel properties, as well as a delivery platform for the controlled release of bioactive molecules and growth factors.

Statement of Significance—One of the major drawbacks associated with the use of conventional hydrogels as carriers of growth factors is their inability to control the release kinetics of the loaded molecules. In fact, in most cases, a burst release is inevitable leading to diminished therapeutic effects and unsuccessful therapies. As a potential solution to this issue, we hereby propose a strategy of incorporating ND complexes within an injectable hydrogel matrix. The functional groups on the surface of the NDs can establish interactions with the model growth factor VEGF and promote a prolonged release from the polymer network, therefore, providing a longer therapeutic effect. Our strategy demonstrates the efficacy of using NDs as an essential

*Corresponding author at: Department of Chemical and Petroleum Engineering, University of Kansas, 4165 C Learned Hall, 1530 W. 15th Street, Lawrence, KS 66045, United States. arghyapaul@ku.edu (A. Paul).

component for the design of a novel injectable nanocomposite system with improved release capabilities.

Keywords

Injectable hydrogel; Sustained release; Nanocomposite hydrogel; Nanomedicine; Bioactive molecules

1. Introduction

Efficient protein-based therapies require the administration of supraphysiological doses of biological molecules, which are necessary to achieve the desired healing response due to their short half-lives and rapid clearance from the body. A common strategy for administering therapeutic proteins is by bolus injection, although this approach has limited clinical success mainly due to possible adverse side effects [1]. For instance, a bolus injection of angiogenic growth factors could be administered to induce revascularization of an ischemic tissue, but due to lack of control over the release, systemic exposure to the growth factor could cause dangerous side effects such as vascular leakage, hypotension, and risk of tumor formation [2]. Similarly, the human bone morphogenetic protein (BMP-2) is an FDA-approved growth factor used for bone regeneration, and it is frequently delivered by bolus injection. Very high doses of BMP-2 must be delivered to observe a therapeutic response *in vivo* because of the short half-life of the protein, which also results in several adverse side effects such as hematoma formation, heterotropic bone growth, and increased postoperative morbidity [3]. These few examples elucidate how fundamental is the design of effective growth factor-based therapies that reduce these side effects by promoting a sustain and localized release of these biological factors within a target tissue [4]. Additionally, controlled release systems can increase the efficacy of these treatments and facilitate a healing response with much lower doses of growth factor required.

Injectable hydrogels represent a valid system that can be utilized for sustained and localized growth factor delivery due to their ease of administration and wide array of customizable properties [5]. Prior to injection, the hydrogel matrix can be loaded with a therapeutic protein and delivered by minimally invasive procedures directly to a site of injury [6–8]. In addition, hydrogel properties vary based on the type of polymer and can also be modulated by the process of crosslinking, which indirectly affects the ability of the hydrogel to swell and degrade [9]. Based on this concept, a variety of systems have been recently investigated, ranging from injectable peptide-based hydrogels [10] to thermo-responsive injectable hydrogels [11–13]. These approaches have been proven to be successful for the design of carriers that can prolong growth factor activity, by preventing degradation or proteolysis and by promoting a localized release to a desired tissue or organ. Moreover, for the treatment of many conditions, such as tissue ischemia, in which multiple injections of growth factors over several time intervals are required to achieve a healing response, an injectable hydrogel platform that requires a single injection is a highly favorable alternative. However, a major drawback associated with traditional hydrogel-based growth factor delivery systems is the limited ability to control the release kinetics of the protein from the hydrogel. When administered *in vivo*, a significant healing response cannot be achieved without precise

control over the release rate to maintain the growth factor concentration at a therapeutic window. The difficulty of designing release platforms that can control both the spatial and temporal release of exogenous growth factors has impeded the use of these technologies in the clinic.

A promising alternative to address this challenge combines nanomaterials with polymers to form injectable nanocomposite hydrogels [14,15]. This design integrates the great advantage of nanoparticles which is the high surface area for adsorption of proteins, along with the ability of the polymeric network to localize the nanoparticles in a target area [16,17]. The choice of a particular nanoparticle can influence the physical and mechanical properties of the hydrogel as well as dictate its ability to retain the loaded growth factor for a prolonged period of time [18]. The nanomaterial can establish a series of interactions at the nanoscale level with both the hydrogel network and the loaded drug, thus influencing the release profile of the protein. The nature of these interactions is strictly correlated with the nanomaterial's properties including surface area, morphology, and the presence of charged or polar functional groups. Several nanomaterials such as clays [19], hydroxyapatite [20], metallic nanoparticles [21] and carbon nanomaterials [12] can be included within the polymeric structure of injectable systems to provide additional properties such as higher mechanical properties or responsiveness to external stimuli. Specifically, among carbon nanoparticles nanodiamonds (NDs) have been recently investigated as an innovative platform to modulate the properties of hydrogels. NDs possess a higher biocompatibility in respect to other widely used carbon-based nanomaterials such as graphene oxide (GO) or carbon nanotubes (CNTs) [22]. Additionally, NDs have high surface area-to-volume ratio which makes them an attractive option as drug nanocarriers for a variety of bioactive molecules including drugs, proteins, DNA, and vaccines [23]. NDs can be embedded within polymeric networks to create nanohybrid systems that display better control over the release kinetics of a loaded growth factor compared to conventional hydrogels.

To test this hypothesis, the current study investigates the influence of NDs on the physical and rheological properties of an injectable growth factor-releasing hydrogel comprised of gelatin and chitosan biopolymers. These two polymers, which crosslink in the presence of β-glycerophosphate (β-GP) and genipin, can gelate at host body temperature (37 °C) making it more suitable for clinical applications. After assessing the biocompatibility of the NDs as nanofillers, further studies examined the potential of NDs to serve as carriers for growth factors by complexation with the model human vascular endothelial growth factor-165 (VEGF). The NDs-VEGF complex was then included in the hydrogel prior to gelation, and the novel injectable nanocomposite system was tested *in vitro* for its ability to modulate the release of VEGF compared to a hydrogel containing the un-complexed protein. Overall, these findings shed light on the importance of NDs as essential nanofillers that can tune the release properties of injectable hydrogels for growth-factor based therapies.

2. Materials and methods

2.1. Injectable hydrogel preparation

Injectable hydrogels were prepared using the following procedure. Firstly, chitosan (3.0% w/v) with a low molecular weight (Mw 10,000 Da) and low degree of acetylation, was

solubilized in CH_3COOH (0.2 N) and mixed with β-GP (20% w/v) to obtain a neutral solution with a pH of 7.4. The final concentration of β-GP in the gel was 2.0% w/v. Secondly, stock solutions of type A gelatin from porcine skin (bloom grade 300) were prepared in deionized water (10 and 20% w/v). The two polymers were mixed in equal volumes to obtain injectable hydrogels containing chitosan (1.5% w/v) and gelatin varying from 2.0% w/v to 4.0% w/v. Hydrogels without gelatin were also prepared and tested as a control group. As a crosslinking agent, genipin was included at a concentration of (0.02% w/v) to facilitate covalent binding in the gelatin-chitosan networks.

2.2. NDs morphology and surface characterization

The morphology and size of the NDs were investigated by transmission electron microscopy (TEM). The TEM samples were prepared by immersing the carbon-coated 200-mesh copper grids into a diluted suspension of NDs (0.25 μg/mL) in deionized water. The grids were subsequently washed with PBS and dried for several hours in a desiccator. The dried grids were analyzed with a Philips CM100 microscope operated at 100 kV. High-resolution TEM was recorded on FEI Tecnai F20XT, 200 kV (FEI, Hilsboro, OR). The hydrodynamic diameter and the zeta potential of the NDs after sonication for 20 min (20 kHz, 2 s on, 1 s off) were measured on a ZetaPALS zeta potential analyzer (Brookhaven Instruments Corporation) by hydrodynamic light scattering and laser Doppler electrophoresis. Finally, the surface chemistry of the NDs was characterized by energy-dispersive X-ray spectroscopy (EDX), and Fourier transform infrared spectra (FTIR) using a Bruker Vector-22 FTIR spectrophotometer (PIKE Technologies, USA). For FTIR spectra analysis ND's powder was mixed in KBr tablet, and spectra were recorded in the range of 400–4000 cm^{-1} (resolution of 1 cm^{-1}).

2.3. Nanocomposite injectable hydrogel preparation

NDs were chosen as the nanomaterial component for the fabrication of the injectable nanocomposite hydrogels. Detonation NDs were purchased from Nanostructured & Amorphous Materials, Inc. (Houston, TX) and used without any further purification from the company. NDs were sonicated for 20 min (20 kHz, 2 s on, 1 s off) in deionized water at a concentration of 0.1% w/v. NDs were then added and thoroughly dispersed in the polymeric mixture prior to the addition of genipin. The concentration of NDs in the hydrogels was varied from 0.005% w/v up to 0.02% w/v while the concentrations of both chitosan (1.5% w/v) and gelatin (2.0% w/v) were kept constant.

2.4. Rheological studies

Rheological studies were conducted to investigate the temperature and time of gelation of the different polymeric mixtures. The rheological characterization was carried out in an AR2000 rheometer (TA Instruments, New Castle, DE). Temperature sweeps were performed at the low oscillation frequency of 1 Hz in the range of 25–40 °C with a temperature increase of 1 °C/min, using a steel cone and plate geometry (cone angle of 2° and diameter of 25 mm). To avoid evaporation during the test, a water trap was placed on the geometry. Different concentrations of gelatin (0, 2.0 and 4.0% w/v) were tested, keeping constant the concentrations of chitosan (1.5% w/v), β-GP (2% w/v), and genipin (0.02% w/v).

In addition, time sweeps at a constant frequency of 1 Hz in the viscoelastic region were then recorded at 37 ° C to evaluate the effect of gelatin concentration on gelation. The same studies were also conducted on samples containing NDs (0.005–0.02% w/v) to investigate whether the nanomaterial was capable of influencing the time of gelation. Both temperature and time sweep were carried out in triplicate using a constant volume of 0.5 mL for each test. Moreover, viscosity measurements were performed on the same solutions and the test was carried out using a cone-plate geometry (cone with 20 mm diameter, 1° angle) in the range of shear rates varying from 0.001 to 1000 s^{-1}. The study was conducted at the temperature of 25 ° C (n = 3).

After hydrogel formation, frequency sweeps in the range from 0.01 up to 10 Hz were recorded for all samples at 37 ° C in the viscoelastic region at 1% of strain defined by a preliminary strain sweep test in the range of 0.1 up to 100% of strain. Injectable hydrogels with and without NDs (1.0 cm in diameter and 0.5 cm height, n = 3) were tested using a 25 mm serrated steel plate-plate geometry, and a water trap was placed on the geometry to avoid evaporation. Finally, recovery studies were carried out at 1 Hz by applying 100% strain for 3 min followed by recovery for 3 min at 1% strain. Hydrogels were swollen before the study by hydration for 1 h in PBS (pH 7.4). Each recovery study was repeated three times.

2.5. Mechanical testing

The compressive modulus of the injectable nanocomposite hydrogels was determined using an RSA-III dynamic mechanical analyzer (TA Instruments, New Castle, DE) and tested under unconfined uniaxial compression with a 35 N load cell (n = 5). The gel diameter was measured with calipers under a stereomicroscope (20X magnification), and the height was measured directly using the RSA-III. All mechanical tests were performed on the swollen injectable nanocomposite hydrogels, and compression plates were lubricated with mineral oil to minimize both any gel plate adhesion and to prevent gel drying during the test. Samples were compressed unconstrained to 95% of their original height or to fracture, which was measured directly with the RSA-III. A compression rate of 0.005 mm/s, corresponding to an average of 15%/min, was used. The compressive modulus (E) was calculated as the slope up to an x-axis value of 10% strain of the stress versus strain curve.

2.6. Physical characterization of the injectable nanocomposite hydrogels

Freeze-dried hydrogels were weighed and soaked in PBS at 37 °C. The equilibrium swelling was evaluated by weighing the swollen hydrogel at different time points, and the swelling ratio (%) was calculated using the following equation (1):

$$Swelling\ ratio\ (\%) = \frac{W_s - W_d}{W_d} \times 100$$

where Ws is the weight of the swollen hydrogel, and W_d represents the weight of the freeze-dried hydrogel. In addition, the porosity of the hydrogel with and without NDs was evaluated by scanning electron microscopy (SEM). Samples were mounted on a holder with

double sided conductive carbon tape and sputter-coated with gold. SEM images were obtained at an acceleration voltage ranging from 1 to 10 kV with an in-lens detector.

Finally, for degradation tests, the freeze-dried hydrogels were weighed and then soaked in a collagenase type IV solution (1 U/ml) dissolved in PBS (pH 7.4). The degradation tests were performed in an incubator at 37.0 °C and 5% CO_2 and the collagenase solution was changed daily. At different time points, the hydrogels were removed from the collagenase solution, washed with PBS, and freeze dried. Five samples were used for each time point of the study, and the percentage of degradation was calculated by weight loss using the following equation (2):

$$W_L\,(\%) = \frac{W_i - W_f}{W_i} \times 100$$

where W_i and W_f are the initial and final weight of the hydrogel after degradation, respectively. Degradation studies were also carried out to test the stability of the nanocomposite hydrogels containing the different concentration of NDs varying from 0.005% w/v up to 0.02% w/v. The study was performed in PBS (pH 7.4) at 37 °C without collagenase shaking the gel at 60 rpm for the duration of 21 days. PBS was replaced every two days, and the test was performed following the same conditions reported above. Additionally, degraded hydrogels at 7 and 21 days were frozen in liquid nitrogen, freeze-dried and imaged with SEM.

2.7. NDs biocompatibility studies

Immortalized human umbilical vein endothelial cells (HUVECs) were cultured in endothelial basal medium (EGM-2 BulletKit, Lonza, 2% Fetal Bovine Serum, and 1% penicillin/streptomycin) with complete endothelial growth supplements at standard culture conditions. HUVECs (between passage 6–9) were used in all the biocompatibility studies. HUVECs were seeded at a density of 1500 cells/cm^2 in a 12 well plate and allowed to grow until they reach confluency. Subsequently, EGM-2 growth media was supplemented with NDs suspension (25 μg/mL) in PBS previously sonicated for 20 min, to study NDs biocompatibility by evaluating the expression of apoptotic genes. As a positive control, camptothecin solution (5 μM) in DMSO/PBS was included to the EGM-2 growth media to induce cell apoptosis [24]. After incubation for 24 h, cells were lysed and apoptotic genes expression was analyzed using the RT-qPCR procedure. mRNA from each group were first extracted using an RNeasy Mini Kit (Qiagen, Germany). mRNA concentrations were measured using a NanoDrop (Thermo Scientific, USA), then normalized to 100 ng of mRNA for its conversion to cDNA. mRNA solutions were converted to cDNA using the High-Capacity cDNA Conversion Kit (Applied Biosystems, USA). All primers used to carry out qPCR analysis were predesigned KiCqStart SYBR Green primers (Sigma-Aldrich, USA). 10 μl of KiCqStart SYBR Green Master Mix was used for each reaction (Sigma-Aldrich, USA). All qPCR reactions were performed using a Mastercycler Realplex4 (Eppendorf, Germany). Fold expression levels were calculated using the relative ΔΔCt method, using GAPDH as the housekeeping gene. To further confirm the NDs' biocompatibility, fluorescence-activated cell sorting (FACS) was carried out to detect the

presence of apoptotic cells after treatment with NDs for 24 h. HUVECs without any treatment and the cells exposed to the drug camptothecin (5 μM) were tested as negative and positive control respectively. Briefly, HUVECs were trypsinized and washed twice with cold PBS. Subsequently, the Annexin V binding buffer was used to resuspend HUVECs (1×10^6 cells/ml). 10 μl of Annexin V-FITC was added to the resuspended HUVECs and incubated for 30 min in the dark, followed by incubation, with 5 μl of propidium iodide (PI) for 10 min. The apoptosis ratio of HUVECs was then immediately measured using the Attune NxT flow cytometer (Thermo-Fischer Scientific, USA).

2.8. Hydrogel biocompatibility studies in vitro

To assess hydrogel biocompatibility, injectable nanocomposite hydrogels were formed in 48 well plate varying the concentration of NDs from 0.005% w/v up to 0.02% w/v. Hydrogels were washed overnight with PBS containing 1% of penicillin/streptomycin and soaked in complete EGM-2 growth media for 1 h. 50×10^3 HUVECs were seeded on each gel and cells were left to grow for 24 h. MTS colorimetric assay (λ = 490 nm) was used to quantify cell viability and assess hydrogel cytotoxicity. Data were reported as the average of five different samples for each group tested. In addition, HUVECs morphology was evaluated at 24 h after seeding. Briefly, samples were stained with a cell-permeant MitoTracker® Red (25 nM) in DMEM media for 30 min to visualize mitochondria. After staining, samples were washed with PBS and fixed in 4% paraformaldehyde. Subsequently, HUVECs were treated with a solution 0.1% Triton X-100 for 20 min followed by staining with Alexa Fluor 488 phalloidin, for visualizing cell cytoskeleton, and DAPI to stain cell nuclei. Fluorescent images were obtained using a spinning disk fluorescent confocal microscope (Olympus IX81/3I).

Additionally, nanocomposite hydrogels were seeded with a murine macrophage cell line (RAW cells) to assess the gene expression of several inflammatory markers. These include the tumor necrosis factor-α (TNF-α), interleukin-6 (IL6), interleukin-1β (IL-1β) and the anti-inflammatory cytokine interleukin 10 (IL10) [25]. Briefly, macrophages were harvested from the gels after 24 h of culture and washed twice with PBS. qPCR analysis of the inflammatory genes was carried out following the same procedure described in the previous section, and the results were determined following the ΔΔCt method.

Finally, the level of activation for several kinase members involved in the mitogen-activated protein kinase (MAPK) pathway was evaluated using western blot analysis [26]. Specifically, the presence of the phospho-P38 mitogen-activated protein kinase (p-P38 MAPK) along with the phospho-extracellular signal-regulated kinase (p-ERK) and the phospho-Jun N-terminal kinase (p-JNK) were investigated. Bone marrow-derived macrophages (BMDM) were seeded on the different nanocomposite hydrogels, and after 24 h cells' lysates were resolved by SDS-PAGE using 10% separating gel under reducing conditions. The resolved proteins were then transferred to polyvinylidene fluoride (PVDF) membranes. The membranes were blocked with LICOR blocking buffer for 1 h followed by incubation overnight at 4 °C with primary antibodies for pERK, p-P38 MAPK, and pJNK (Cell Signaling Technology, USA). All the primary antibodies were previously diluted to 1:1000 using the blocking buffer. Then, the membranes were washed three times and

incubated with the LICOR-conjugated goat anti-rabbit secondary antibody. Protein bands for p-P38, p-ERK, and p-JNK were detected using a LiCor Odyssey scanner system and analyzed using ImageJ. The intensity of each band relative to the phosphorylated protein was normalized to the band intensity obtained from its respective loading control non-phosphorylated. Data are expressed as mean value ± deviation standard (n = 3).

2.9. Evaluation of the biocompatibility and biodegradability of the nanocomposite hydrogels in vivo

Male Wistar rats (n = 3), were housed in the animal care facility and all experiments were carried out according to the NIH “Guide for the Care and Use of Laboratory Animals”. The study was approved by the Institutional Animal Care and Use Committee, University of Cincinnati. Prior to subcutaneous implantation, the animals were subjected to general anesthesia with isoflurane and carprofen-based analgesia. Then, the dorsal skins of the rats were incised to form subcutaneous pockets where the nanocomposite hydrogels were placed. Prior to implantation, the hydrogels without NDs and the nanocomposite system having NDs at the concentrations 0.01% w/v were fabricated in 24 well plate in sterile conditions and washed thoroughly with PBS (pH 7.4) containing penicillin/streptomycin 1% w/v. Seven and twenty-one days after wound closure, the animals were euthanized, and the adjacent subcutaneous tissue around the hydrogels was explanted. The hydrogels were embedded in O.C.T. and frozen at 80 °C. Hematoxylin/eosin (H&E) staining were performed on 6 mm cryosections of the frozen tissues according to standard protocols [27,28].

2.10. Evaluation of HUVECs traction forces on the nanocomposite hydrogels

The injectable nanocomposite hydrogels were fabricated in combination with fluorescent microbeads (Fisher Scientific, USA) having a diameter of 0.2 μm, to examine the influence of the substrate stiffness on HUVECs traction forces on the gels. Microbeads were homogeneously dispersed in the polymeric mixture by vortexing them for five minutes. Then, each hydrogel was prepared by adding 45 μl of the sample on a petri-dish in between two spacers with a desirable height of 50 μm. The drop was flattened between the spacer using a glass slide previously coated with 3-tri(methoxysilyl)propyl methacrylate (TMSPMA) (Sigma, USA). After gel formation at 37 °C the glass slides containing the gels were washed with PBS and soaked in complete EGM-2 growth media for two hours. HUVECs (5×10^3 cells for each gel) were seeded and kept growing for 24 h. Cells were removed from the gel using trypsin after 24 h. Fluorescent images of the beads before and after the step of cell removal were taken for the same field of view using an EVOS cell imaging microscope (Thermo-Fischer Scientific, USA). The displacement caused by each cell’s traction forces was calculated by comparing the fluorescent positions of the beads between the two sets of images relative to the gels in the stressed and relaxed state. The root mean square (RMS) traction was calculated using Matlab (Mathwork Inc.) and obtained from the displacement field, taking into consideration the values of compressive elastic modulus for each hydrogel substrate [29].

2.11. ND/VEGF complex formation and characterization

NDs were dispersed in deionized water (10 mg/mL) and sonicated for 30 min (20 kHz, 2 s on, 1 s off) with an Ultrasonic Processor 500W Ultrasonic, 20 kHz (Midwest Scientific, Inc.,

St. Louis, MO). Subsequently, 0.5 mL of the nanosuspension was mixed with an equal volume of a solution of VEGF (100 ng/mL) prepared in phosphate buffer at pH 7.4. The ratio between ND and VEGF was chosen according to similar studies based on the complexation of NDs with other angiogenic growth factors [30,31]. Then, the mixture was shaken at 60 rpm overnight at 37 °C followed by centrifugation for 20 min at 14,000 rpm. The pellet containing the ND/VEGF complex was either resuspended in water or dried for further characterization through TEM, EDX and FT-IR spectroscopy. ELISA quantification of VEGF was carried out to assess the amount of VEGF adsorbed on the surface of the NDs, which was determined considering the difference in the protein content pre- and post-centrifugation in the supernatant. The % of growth factor adsorbed was calculated as mean ± deviation standard (n = 6). Additionally, ELISA quantification was carried out testing a solution of VEGF (100 ng/mL) in phosphate buffer without NDs pre and post-centrifugation in the same condition used for the preparation of the complex. This test was necessary to determine whether the process of centrifugation was causing any reduction in the content of protein in solution as free growth factor and to verify the selectivity of the centrifugation step as technique to separate only the ND/VEGF complex.

2.12. In vitro VEGF release study

The ND-VEGF complex, obtained as a pellet after centrifugation, was resuspended in 200 μL of deionized water and mixed with the polymeric mixture to reach a final volume of 1 mL containing chitosan (1.5% w/v), gelatin (2.0% w/v), β-GP (2% w/v) and genipin (0.02% w/v). Similarly, VEGF as free growth factor was added to the polymeric mixture prior to gelation and the concentration of VEGF was chosen based on the amount of protein adsorbed on the NDs. Briefly, 400 μL of each gel was placed into 48-well plates and allowed to form a gel at the bottom of each well. All wells were then filled with 200 μL of PBS and the release was carried out at 37 °C while shaking orbitally at 60 rpm. The entire volume was withdrawn at different time intervals and replaced with PBS each time. The amount of VEGF released was quantified by ELISA and using a standard calibration curve in the range from 32 pg/mL to 1 ng/mL. The percentage of growth factor released was reported as the average ± deviation standard (n = 3). The experimental data were fit to the Korsmeyer-Peppas model, which is a semi-empirical model that was developed to model drug release from a polymeric matrix such as a hydrogel. While this model does not indicate the specific release mechanism of a system, it can be used to identify the presence of anomalies or deviations from Fickian diffusion. The Korsmeyer-Peppas model is based upon the power law equation (3):

$$\frac{M_t}{M_\infty} = kt^n$$

where M_t and M_∞ are the cumulative concentrations of drug released at time t and at time infinity, respectively. In addition, k is the release rate constant which depends upon the geometry and structure of the matrix and n is the release exponent which is used to characterize the release mechanism. If n = 1, the release is zero order, if n = 0.5, the release is best described by Fickian diffusion, and 0.5 < n < 1 indicates anomalous transport [32].

Finally, to test whether the released VEGF from the nanocomposite hydrogel was still active a proliferation study was carried out *in vitro*. Briefly, HUVECs (10×10^3) were seeded in a 96 well plate and allowed to adhere for 3 h in EGM-2 media without basic fibroblast growth factor (bFGF) and VEGF. Then, the media was supplemented with the VEGF released from the nanocomposite hydrogels at 96 h and cells were allowed to proliferate for 48 h. As positive and negative control HUVECs were cultured for 48 h in complete Lonza Media and without bFGF and VEGF, respectively. For each group five different wells were tested. Then, MTS colorimetric assay ($\lambda = 490$ nm) was used to quantify the proliferation of HUVECs in the different groups at 48 h. The number of HUVECs was determined using a standard curve in the range from 1×10^3 to 2×10^4 cells and the results were expressed as mean ± deviation standard (n = 5).

2.13. Statistical analysis

Statistical analysis was performed using one-way analysis of variance (ANOVA) followed by Tukey's multiple comparison test used to determine whether a significant difference exists between specific groups. All statistical analyses were carried out with Graphpad Prism Software 6. A p value less than 0.05 indicates statistical significance, which was displayed as * = $p < 0.05$, ** = $p < 0.01$, *** = $p < 0.001$.

3. Results

3.1. Hydrogel formation and characterization

The hydrogel was designed by combining chitosan and gelatin with two crosslinkers, genipin and beta-glycerophosphate (β-GP), to ensure the formation of a thermosensitive injectable hydrogel (Fig. 1A). All of the gels exhibited sol-gel transition at 35–39 °C, which was confirmed by the decrease in tan δ (G''/G') (Fig. 1B). The group formed without β-GP, on the other hand, showed a solution behavior at all tested temperatures. While the addition of gelatin at 2% w/v did not alter the sol-gel transition, the values of tan δ were observed to decrease prior gelation, which is indicative of the formation of electrostatic interactions between the two polymers. Furthermore, the presence of gelatin at 2% w/v did not alter the gelation temperature (Fig. S1A–C), but it did reduce the gelation time by 40% at the conditions tested (Fig. 1C). Gelatin at concentrations above 2% w/v did not affect the gelation time (Fig. S1D). Additionally, gelatin is essential for the fabrication of stiffer gels with higher values of G' as observed in the frequency sweeps performed on the hydrogels (Fig. 1D). Similarly, hydrogels formed with gelatin at 4% w/v exhibited the highest compressive stress up to 380 ± 10 kPa compared to the control composed only of chitosan, which displayed a compressive stress of 12 ± 5 kPa and lower strain at the point of breakage (Fig. 2A). No significant change was detected in the compressive Young's Modulus as the concentration of gelatin was varied up to 4% w/v (Fig. 2B). Aside from the mechanical and rheological behavior, gelatin also had an impact on the physical properties of the injectable hydrogels. The presence of gelatin modified the degree of swelling compared to the system made of chitosan only (Fig. 2C). The degradability of the different formulations in collagenase solution was greatly affected by the concentration of gelatin. Hydrogels containing 4% w/v of gelatin completely degraded after 96 h in comparison to the control gels formed with chitosan, which showed only 50% degradation over the same timeframe

(Fig. 2D). Since the changes in gelation time and mechanical properties were not favorable in gels formed with gelatin at 4% w/v, the group containing 2% w/v gelatin was selected for further testing and optimization of the nanocomposite hydrogels.

3.2. Effect of NDs on hydrogel properties

To create the nanocomposite hydrogels, detonation NDs with a mean diameter of 220 nm and ζ-potential of −9.4 ± 0.9 were thoroughly dispersed at different concentrations in the polymeric mixture prior to gelation (Fig. 3A). FT-IR of NDs revealed the presence of hydroxyl (3421 cm^{-1}, ν O–H), alkyl (2917 cm^{-1}, ν C–H), and carbonyl groups (1714 cm^{-1}, ν C=O) which establish hydrogen bonds and dipole-dipole interactions with the polymeric mixture (Fig. S2A). The shape of detonation NDs was irregularly spherical with a size less than 20 nm (Fig. S2B). The addition of NDs did not affect the gelation time or the initial viscosity of the solution prior to gelation which was around 100 Pa.s. Additionally, the internal morphology of the gel was not influenced by the presence of NDs as displayed by SEM images (Fig. S2B–D). However, the interactions between NDs and the hydrogel network were apparent by the resulting changes in hydrogel stiffness. In comparison with the gel without NDs, which displayed a Young's modulus of 6.3 ± 0.2 kPa, the gel formed with NDs at a concentration of 0.01% w/v displayed a higher Young's modulus of 7.3 ± 0.4 kPa. The observed increase in Young's modulus can be attributed to the interactions between the polar functional groups of the NDs and the polymeric matrix (Fig. 3B). When gels were formulated with ND concentrations above 0.01% w/v though, the same trend was not observed, which concludes that the NDs had a concentration-dependent effect on the mechanical properties of the hydrogel but only within a precise range of concentrations. Furthermore, the injectable nanocomposite hydrogel was subjected to different strain oscillatory cycles and displayed over 95% recovery of its original storage modulus (G′). Higher G′ values were observed in the gel with 0.01% w/v NDs (Fig. 3C). NDs were found to have an impact on the physical properties of the hydrogels, based on the observed trend of increased swelling with increased ND concentration. A probable theory that elucidates this trend is that the increase in ND concentration leads to an abundance of polar functional groups in the gel, which enables the gel to uptake a greater volume of water (Fig. 3D).

3.3. Investigation of the biocompatibility of NDs and the nanocomposite hydrogels in vitro and in vivo

Preliminary studies investigated the biocompatibility of NDs by evaluating the expression of apoptotic genes *in vitro* in HUVECs treated with NDs at a concentration of 25 μg/mL for 24 h. All the genes studied with qPCR such as BID, BAX, BAK, BAD and BBC3 were downregulated in comparison to the positive control, which consisted of HUVECs treated with 5 μM camptothecin (Fig. S3A). FACS analysis was also conducted to confirm the qPCR results. Briefly, HUVECs were treated with NDs as previously mentioned, and after 24 h the cells were stained with annexin V, which enabled the quantification of apoptotic cells. The difference in the number of apoptotic cells between the experimental group and control group was negligible (Fig. S3B).

After confirming that the NDs did not cause any cytotoxic effects, the biocompatibility of the nanocomposite hydrogel was assessed by seeding HUVECs onto hydrogels with a range

of increasing ND concentration. Upon incubation for 24 h, an MTS assay verified that each experimental hydrogel group was biocompatible, and the presence of NDs did not impact the cell viability (Fig. 4A). HUVECs were able to adhere and proliferate on the surface of the nanocomposite hydrogels after 24 h (Figs. 4B and S4). Further analysis concluded that the NDs at a concentration of 0.01% w/v did not disrupt the mechanical forces that the cell exerted on the hydrogel surface (Fig. 4C–D).

To determine the presence of an inflammatory response that could be induced by the NDs in the nanocomposite gel, gene expression of inflammatory markers such as TNFα, IL1β, IL6 and the anti-inflammatory cytokine IL10 in RAW macrophage cells were tested with qPCR. Inclusion of NDs at all tested concentrations did not affect the expression levels of inflammatory cytokines in comparison with control gels formed without NDs (Fig. 4E). Interestingly, the expression of the anti-inflammatory gene IL10 was proportional to the concentration of NDs up to 0.02% w/v in comparison to the control hydrogel lacking NDs (Fig. 4F). The activation of MAPK was also investigated by western blot analysis on the macrophage lysate to determine the expression levels of p-P38, p-ERK, and p-JNK. The presence of NDs upregulated the production of these phosphorylated proteins irrespective of the ND concentration (Fig. S5 A–D).

Additionally, the NDs effect on the hydrogel stability was investigated. NDs at the concentration of 0.01% w/v improved the stability of the hydrogels after being exposed to PBS for 7 and 14 days respectively. However, no significant change in the mass loss and morphology among the groups was found after 21 days (Fig. 5AB). Finally, the hydrogels were also tested for their biocompatibility and biodegradability *in vivo* after subcutaneous implantation in rats. As observed in the *in vitro* study, the gel showed good biocompatibility with minimal signs of inflammation in the surrounding tissue after 21 days. No infiltration of inflammatory cells was evident in the hydrogels' network (Fig. 5C), and both systems were capable of integrating within the host tissue. The hydrogels with and without NDs were still present after 21 days although the internal structure of the network in both systems started to lose its integrity in accordance with the results observed *in vitro.*

3.4. Formation of ND-VEGF complexes and VEGF release studies

NDs in suspension at 0.01% w/v was incubated with VEGF (100 ng/mL) in PBS for 24 h, which resulted in the adsorption of the growth factor to the surface of the NDs forming the ND-VEGF complex (Fig. 6A). The ratio between NDs and VEGF was optimized based on previous studies reporting the complexation of NDs with angiogenic growth factors such as angiopoietin 1 and VEGF [31]. The loading efficiency of protein adsorption was analyzed by conducting VEGF ELISA on the aqueous suspension prior to and 24 h after mixing with NDs. The percentage of protein adsorbed onto the surface of NDs was 91.2% ± 2.6% (n = 6) of the original amount of growth factor. The FTIR spectra of the ND-VEGF complex presented both the characteristics peaks associated with NDs and with VEGF. In addition to the main peaks associated with NDs including the hydroxyl (3421 cm^{-1}, ν O–H), alkyl (2917 cm^{-1}, ν C–H), and carbonyl peaks (1714 cm^{-1}, ν C=O) the peak that is unique to the spectra for VEGF, which is the disulfide bond (547 cm^{-1}, ν S–S), was also observed in the ND-VEGF complex (Fig. 6B). EDX analysis of ND-VEGF revealed the presence of

nitrogen and sulfur which were absent in the EDX spectra of NDs, thus confirming the presence of VEGF on the surface of NDs (Fig. 6C).

To form the injectable nanocomposite hydrogel, ND-VEGF complexes were included in the polymeric mixture prior to gelation. To assess the release of VEGF from the nanoparticle complexes, hydrogels were also formed with unmodified VEGF to serve as a control. The control gel exhibited first order release kinetics by the diffusion of VEGF which occurred over a 96 h time period (Fig. 6D). On the other hand, the hydrogels containing ND-VEGF exhibited sustained release of VEGF with complex kinetics, and after 96 h only 40% of the loaded VEGF was released from the hydrogel. In both the control gels containing VEGF and the experimental hydrogels containing ND-VEGF, a biphasic release profile was observed, with an initial burst release of VEGF for the first 12 h followed by a slower release for the remainder of the study. After 5 days, the release of VEGF from both control and experimental gels appeared to reach a constant rate, indicated by the plateau of the release profile. These results suggest that the hydrogel itself may have had a role in facilitating sustained release of the protein, regardless of whether or not it was contained within a nanoparticle complex. To model the release of VEGF, the release profiles for both hydrogels were fit to the Korsmeyer-Peppas model. According to the Korsmeyer-Peppas model, the release exponent corresponding to the control gel with free VEGF was $n = 0.47$, indicative of Fickian diffusion. On the contrary, the release exponent for the experimental gel containing ND-VEGF complex was $n = 0.57$, which indicates that the release follows non-Fickian behavior, revealing that additional transport phenomena are introduced with the complexation of the protein with NDs (Fig. 6D). All the kinetics parameters for the two systems are summarized in Table 1.

To verify the bioactivity of the released VEGF and ensure that the complexation with NDs did not degrade the protein, HUVECs were exposed to the supernatant containing the VEGF released at 96 h. After 48 h of incubation, an MTS assay was conducted to evaluate cell viability and growth. VEGF and bFGF, which are normally combined with HUVEC culture media as growth supplements, were not added to the media. The MTS assay confirmed the bioactivity of the released growth factor that was able to promote cell growth similarly to the supplemented media (Fig. 6E).

4. Discussion

As the first part of our investigation, it was essential to optimize the parameters required for the formation of an injectable hydrogel that can be administered at room temperature and form a gel around 37 °C. To address this challenge, the hydrogel was formulated using a combination of chitosan and β-GP that can form a thermo-sensitive system according to the pH and the polymer concentration [33,34]. In our study, the concentration of chitosan was kept constant while the amount of β-GP was optimized to bring the pH of the polymeric solution up to 7.4 and promote the sol gel transition of the chitosan solution at 37 °C. Genipin was kept constant at 0.02% w/v in all the systems investigated to ensure the formation of covalent bonds between gelatin and chitosan polymeric chains and to reinforce the hydrogel. Higher concentration of genipin would have reduced the gelation time but this option was not ideal as too much crosslinker would have completely compromised the

biological activity of the loaded growth factor. For this reason to reduce the time of gelation several concentration of gelatin were tested and better results were observed working at 2% w/v of gelatin. Gelatin influenced the mechanical properties of the hydrogel by increasing the storage modulus of the gel (G′) and the compressive modulus without altering its thermosensitive property. The observed effect of gelatin was similar to other previous attempts reported in the literature which investigated chitosan gelatin systems for a variety of other biomedical applications such as replacement for load-bearing soft tissue [35–37]. However, it is important to underline that the parameters optimized in this study may change according to a variety of factors including the degree of deacetylation and molecular weight of chitosan and type of gelatin used. For this reason, the results reported here are valid only if all these other factors are taken into consideration.

To further extend the utility of this optimized system as carrier for growth factors it was important to introduce a nanomaterial capable of influencing the final properties of the injectable hydrogel. NDs were selected to serve this purpose due to their well-known ability to adsorb drugs and proteins and modulate their release [38–40]. In addition, the presence of polar functional groups on their surface can establish interactions within the polymeric chains and alter the physical and mechanical properties of our designed injectable system. The NDs used in this study are detonation NDs which possess a heterogeneous composition of polar functional groups on their surface. The main functionalities are hydroxyl groups and carbonyl groups as evidenced by FTIR spectroscopy which can establish dipole-dipole interactions and hydrogen bonds with both polymers. The small increase in stiffness observed can be attributed to the lack of charged groups on the NDs' surface which would have caused a higher increase in the hydrogel stiffness as reported in other studies [41]. Interestingly, the inclusion of NDs did not hamper the gelation time suggesting how the process of gel formation is not affected by the nanomaterial.

NDs were also selected in the design of this carrier due to their low toxicity compared to other carbon nanomaterials such as graphene oxide or carbon nanotubes [42–44]. To confirm this statement, we carried out *in vitro* cytotoxicity tests on HUVECs and our findings confirmed the biocompatibility of the NDs since they were not able to induce an apoptotic effect on HUVECs after being exposed for 24 h at the concentration of 25 μg/mL. Our results suggest an absence of apoptotic effect in the condition investigated, however similar studies showed that the time of exposure and the concentration of NDs are essential variables that can cause an increase in the production of radical oxygen species (ROS) and induce apoptosis in HUVECs [45].

Moreover, it was fundamental to assess the biocompatibility of the injectable nanocomposite systems. For this reason, both HUVECs viability and morphology were investigated in 2D and no significant reduction in cell viability was observed for all the concentration of NDs tested. Moreover, the inclusion of NDs within the hydrogel did not cause any increase in the gene expression of several inflammatory cytokines including TNF-α, IL1-β, and IL-6 while the expression of the anti-inflammatory IL-10 was higher in the group containing NDs. The designed platform was also biocompatible *in vivo* as no sign of inflammatory cell infiltration was evidenced in the gels after 21 days after subcutaneous implantation.

Finally, as a major focus of the current study, the loading and release of the angiogenic growth factor VEGF from the injectable nanocomposite hydrogel was investigated, and the utility of detonation NDs as a sustained release platform for VEGF was assessed. When delivered to the human body by bolus injection, VEGF has a half-life of only 30 min [46]. Due to its short half-life and rapid clearance, large doses of growth factor must be delivered by bolus injection to achieve a desired therapeutic response which are often accompanied by adverse side effects resulting from the high dose. The objective of this study was to present a solution to the aforementioned issue, by developing a nanocomposite hydrogel that provides a sustained and localized release of VEGF. By loading VEGF in a nanoparticle carrier, the resulting sustained release allows for much lower doses to achieve a therapeutic response, in comparison to bolus injection. By further incorporating NDVEGF complexes in an injectable hydrogel, a potential treatment platform for conditions such as myocardial ischemia is presented, and the nanocomposite hydrogel facilitates both the localized and sustained release of growth factor to the site of implantation. To achieve this goal, we demonstrated the efficient adsorption of VEGF onto the surface of NDs to form ND-VEGF complexes, following a previously established protocol for linking NDs with BMP-2 [47]. The formation of the ND-VEGF complex was verified by several techniques including EDX analysis, FT-IR spectroscopy and quantification of unbound protein by ELISA. The ND-VEGF complex was mainly possible due to the formation of hydrogen bonds, dipole-dipole, and hydrophobic adsorption since no carboxylic or amines groups are present in the NDs used in this study. Alternatively, the introduction of these functional groups on the NDs' surface would have been useful to form electrostatic interactions with VEGF and increase the stability of the complex. For instance, the heparin binding site of $VEGF_{165}$ possesses a highly positively charged heparin binding domain at the carboxyl terminal composed of lysines and arginines that could establish electrostatic interactions with negatively charged groups on the surface of NDs [48]. Once the complex was characterized, it was incorporated into a polymeric network of chitosan and gelatin to develop an injectable polymeric scaffold that provided a controlled release of VEGF. In comparison to the control hydrogel loaded with VEGF which released all of the loaded protein within 96 h, the hydrogel loaded with ND-VEGF complexes displayed a continued release of VEGF at a reduced level beyond 96 h. The release profiles of the control hydrogel loaded with VEGF and the experimental hydrogel loaded with ND-VEGF were both compared to modeled profiles generated by the Korsmeyer-Peppas equation to gain further insight on the mass transport mechanisms involved in the release of VEGF [32]. The Korsmeyer-Peppas equation was used to model the release profiles of both systems, and the regressed release exponent was used to classify the release behavior. A release exponent of 0.5 designates Fickian diffusion, and a value above 0.5 indicates anomalous transport, or non-Fickian diffusion. The release profile corresponding to the control hydrogel was fit with a release exponent of 0.47, indicating Fickian diffusion. On the contrary, the n value obtained for the system loaded with ND-VEGF was equal to 0.57 which is indicative of non-Fickian diffusion. While further experimental work is necessary to elucidate the specific transport phenomena involved, it is possible to conclude that the interaction between the NDs and VEGF can be responsible for the sustained release of VEGF. Furthermore, the bioactivity of the VEGF was unaffected by the complexation process, as the VEGF released from NDVEGF complexes induced HUVEC proliferation to the same degree as unmodified VEGF. Together, these results

validated our hypothesis that NDs can serve as biocompatible carriers for growth factors such as VEGF and therefore can prolong the retention of VEGF within an injectable hydrogel. Based upon the success in the current study, the same strategy could be applied to many other types of growth factors to facilitate their sustained release to address a variety of therapeutic applications. In fact, NDs have been already investigated as nanocarrier for the complexation of other proteins such as BMP-2 [47,49], bFGF [47], and angiopoietin-1 [50].

Overall these findings suggest that NDs can not only be incorporated into a hydrogel as a nanofiller to enhance the mechanical properties but they can also non-covalently link with VEGF and provide sustained release of angiogenic growth factor from the hydrogel. However, future work to progress this technology toward potential clinical translation as wound healing system includes optimizing the release profile of VEGF to achieve concentrations that will invoke a healing response, as well as evaluating the therapeutic efficacy *in vivo* in a small animal model. Moreover, to be effective the designed nanocomposite hydrogel should be able to modulate the release of multiple growth factors involved in the process of wound healing including platelet-derived growth factor (PDGF) and transforming growth factor-β (TGF-β) [51,52].

5. Conclusion

A novel injectable thermosensitive nanocomposite hydrogel composed of chitosan, gelatin and nanodiamonds has been investigated as a promising carrier for the sustained delivery of VEGF. The presence of NDs within the polymeric matrix was able to modulate the mechanical properties of the injectable hydrogel without altering the time and the temperature of gelation. Additionally, NDs did not cause any cytotoxic effect or any adverse inflammatory response *in vitro* which are both important aspects to consider for the design of a novel carrier for growth factor based therapy.

Finally, NDs were able to form a complex with VEGF and the inclusion within the hydrogel enabled a sustained release of VEGF which was still active as demonstrated by *in vitro* proliferation studies. Overall these results suggest how the addition of NDs is a useful strategy to design novel carrier with improved release capabilities for growth factor bases therapies.

Supplementary Material

Refer to Web version on PubMed Central for supplementary material.

Acknowledgments

The authors acknowledge the University of Kansas for funding and assistance which made possible the realization of this research project. A.P. acknowledges an investigator grant provided by the Institutional Development Award (IDeA) from the National Institute of General Medical Sciences (NIGMS) of the NIH Award Number P20GM103638.

Additionally, the authors would like to acknowledge the financial support obtained from The Post-Baccalaureate Research Education Program (PREP) which is sponsored by the National Institute of Health (NIH). The authors would like to thank Kartikeya Singh Jodha and Divya Murali for their help provided in the initial part of the project and Dr. Prem Thapa and Ms. Heather Shinogle of the University of Kansas Microscopy and Analytical Imaging Laboratory for their constant assistance with confocal fluorescence microscopy, TEM and SEM imaging. Finally,

the authors would like to thank Prof. Stevin Gehrke and Prof. Michael Detamore for allowing the use of their laboratory equipment to carry out this work.

References

1. Lazarous DF, Shou M, Stiber JA, Dadhania DM, Thirumurti V, Hodge E, Unger EF. Pharmacodynamics of basic fibroblast growth factor: route of administration determines myocardial and systemic distribution. Cardiovasc Res. 1997; 36(1):78–85. [PubMed: 9415275]
2. Hariawala MD, Horowitz JR, Esakof D, Sheriff DD, Walter DH, Keyt B, Isner JM, Symes JF. VEGF improves myocardial blood flow but produces EDRF-mediated hypotension in porcine hearts. J Surg Res. 1996; 63(1):77–82. [PubMed: 8661176]
3. James AW, LaChaud G, Shen J, Asatrian G, Nguyen V, Zhang X, Ting K, Soo C. A review of the clinical side effects of bone morphogenetic protein-2. Tissue Eng Part B Rev. 2016; 22(4):284–297. [PubMed: 26857241]
4. Lee K, Silva EA, Mooney DJ. Growth factor delivery-based tissue engineering: general approaches and a review of recent developments. J R Soc Interface. 2011; 8(55):153–170. [PubMed: 20719768]
5. Silva EA, Mooney DJ. Spatiotemporal control of vascular endothelial growth factor delivery from injectable hydrogels enhances angiogenesis. J Thromb Haemost: JTH. 2007; 5(3):590–598. [PubMed: 17229044]
6. Bae KH, Wang LS, Kurisawa M. Injectable biodegradable hydrogels: progress and challenges. J Mater Chem B. 2013; 1(40):5371–5388.
7. Yang JA, Yeom J, Hwang BW, Hoffman AS, Hahn SK. In situ-forming injectable hydrogels for regenerative medicine. Prog Polym Sci. 2014; 39(12):1973–1986.
8. Lum L, Elisseeff J. Injectable hydrogels for cartilage tissue engineering. Top Tissue Eng. 2003:1–25.
9. Tan H, Li H, Rubin JP, Marra KG. Controlled gelation and degradation rates of injectable hyaluronic acid-based hydrogels through a double crosslinking strategy. J Tissue Eng Regenerative Med. 2011; 5(10):790–797.
10. Martin C, Oyen E, Mangelschots J, Bibian M, Ben Haddou T, Andrade J, Gardiner J, Van Mele B, Madder A, Hoogenboom R, Spetea M, Ballet S. Injectable peptide hydrogels for controlled-release of opioids. MedChemComm. 2016; 7(3):542–549.
11. Boere KWM, Soliman BG, Rijkers DTS, Hennink WE, Vermonden T. Thermoresponsive injectable hydrogels cross-linked by native chemical ligation. Macromolecules. 2014; 47(7):2430–2438.
12. Paul A, Hasan A, Kindi HA, Gaharwar AK, Rao VTS, Nikkhah M, Shin SR, Krafft D, Dokmeci MR, Shum-Tim D, Khademhosseini A. Injectable graphene oxide/hydrogel-based angiogenic gene delivery system for vasculogenesis and cardiac repair. ACS Nano. 2014; 8(8):8050–8062. [PubMed: 24988275]
13. Hasan A, Khattab A, Islam MA, Hweij KA, Zeitouny J, Waters R, Sayegh M, Hossain MM, Paul A. Injectable hydrogels for cardiac tissue repair after myocardial infarction. Adv Sci. 2015; 2(11) n/a-n/a.
14. Whitlow J, Pacelli S, Paul A. Polymeric nanohybrids as a new class of therapeutic biotransporters. Macromol Chem Phys. 2016; 217(11):1245–1259.
15. Paul A. Nanocomposite hydrogels: an emerging biomimetic platform for myocardial therapy and tissue engineering. Nanomedicine. 2015; 10(9):1371–1374. [PubMed: 25996115]
16. Li X, Chen S, Zhang B, Li M, Diao K, Zhang Z, Li J, Xu Y, Wang X, Chen H. In situ injectable nano-composite hydrogel composed of curcumin, N,O-carboxymethyl chitosan and oxidized alginate for wound healing application. Int J Pharm. 2012; 437(1–2):110–119. [PubMed: 22903048]
17. Wang Q, Wang Q, Teng W. Injectable, degradable, electroactive nanocomposite hydrogels containing conductive polymer nanoparticles for biomedical applications. Int J Nanomed. 2016; 11:131–145.
18. Appel EA, Tibbitt MW, Webber MJ, Mattix BA, Veiseh O, Langer R. Self-assembled hydrogels utilizing polymer–nanoparticle interactions. Nat Commun. 2015; 6

19. Gaharwar AK, Avery RK, Assmann A, Paul A, McKinley GH, Khademhosseini A, Olsen BD. Shear-thinning nanocomposite hydrogels for the treatment of hemorrhage. ACS Nano. 2014; 8(10):9833–9842. [PubMed: 25221894]
20. Wang Q, Gu Z, Jamal S, Detamore MS, Berkland C. Hybrid hydroxyapatite nanoparticle colloidal gels are injectable fillers for bone tissue engineering. Tissue Eng Part A. 2013; 19(23–24):2586–2593. [PubMed: 23815275]
21. Campbell S, Maitland D, Hoare T. Enhanced pulsatile drug release from injectable magnetic hydrogels with embedded thermosensitive microgels. ACS Macro Lett. 2015; 4(3):312–316.
22. Zhu Y, Li J, Li W, Zhang Y, Yang X, Chen N, Sun Y, Zhao Y, Fan C, Huang Q. The biocompatibility of nanodiamonds and their application in drug delivery systems. Theranostics. 2012; 2(3):302–312. [PubMed: 22509196]
23. Mochalin VN, Shenderova O, Ho D, Gogotsi Y. The properties and applications of nanodiamonds. Nat Nanotechnol. 2012; 7(1):11–23.
24. Simak J, Holada K, Vostal JG. Release of annexin V-binding membrane microparticles from cultured human umbilical vein endothelial cells after treatment with camptothecin. BMC Cell Biol. 2002; 3:11. [PubMed: 12052248]
25. Thangavel J, Malik AB, Elias HK, Rajasingh S, Simpson AD, Sundivakkam PK, Vogel SM, Xuan YT, Dawn B, Rajasingh J. Combinatorial therapy with acetylation and methylation modifiers attenuates lung vascular hyperpermeability in endotoxemia-induced mouse inflammatory lung injury. Am J Pathol. 2014; 184(8):2237–2249. [PubMed: 24929240]
26. Thangavel J, Samanta S, Rajasingh S, Barani B, Xuan YT, Dawn B, Rajasingh J. Epigenetic modifiers reduce inflammation and modulate macrophage phenotype during endotoxemia-induced acute lung injury. J Cell Sci. 2015; 128(16):3094–3105. [PubMed: 26116574]
27. Paul A, Manoharan V, Krafft D, Assmann A, Uquillas JA, Shin SR, Hasan A, Hussain MA, Memic A, Gaharwar AK, Khademhosseini A. Nanoengineered biomimetic hydrogels for guiding human stem cell osteogenesis in three dimensional microenvironments. J Mater Chem B, Mater Biol Med. 2016; 4(20):3544–3554. [PubMed: 27525102]
28. Waters R, Pacelli S, Maloney R, Medhi I, Ahmed RP, Paul A. Stem cell secretome-rich nanoclay hydrogel: a dual action therapy for cardiovascular regeneration. Nanoscale. 2016; 8(14):7371–7376. [PubMed: 26876936]
29. Butler JP, Tolic-Norrelykke IM, Fabry B, Fredberg JJ. Traction fields, moments, and strain energy that cells exert on their surroundings. Am J Physiol Cell Physiol. 2002; 282(3):C595–605. [PubMed: 11832345]
30. Moore L, Gatica M, Kim H, Osawa E, Ho D. Multi-protein delivery by nanodiamonds promotes bone formation. J Dent Res. 2013; 92(11):976–981. [PubMed: 24045646]
31. Schimke MM, Stigler R, Wu X, Waag T, Buschmann P, Kern J, Untergasser G, Rasse M, Steinmüller-Nethl D, Krueger A, Lepperdinger G. Biofunctionalization of scaffold material with nano-scaled diamond particles physisorbed with angiogenic factors enhances vessel growth after implantation. Nanomed: Nanotechnol Biol Med. 2016; 12(3):823–833.
32. Costa P, Sousa Lobo JM. Modeling and comparison of dissolution profiles. Eur J Pharm Sci. 2001; 13(2):123–133. [PubMed: 11297896]
33. Kim S, Nishimoto SK, Bumgardner JD, Haggard WO, Gaber MW, Yang Y. A chitosan/β-glycerophosphate thermo-sensitive gel for the delivery of ellagic acid for the treatment of brain cancer. Biomaterials. 2010; 31(14):4157–4166. [PubMed: 20185170]
34. Zhou HY, Jiang LJ, Cao PP, Li JB, Chen XG. Glycerophosphate-based chitosan thermosensitive hydrogels and their biomedical applications. Carbohydr Polym. 2015; 117:524–536. [PubMed: 25498667]
35. Sarem M, Moztarzadeh F, Mozafari M. How can genipin assist gelatin/carbohydrate chitosan scaffolds to act as replacements of load-bearing soft tissues? Carbohydr Polym. 2013; 93(2):635–643. [PubMed: 23499106]
36. Chiono V, Pulieri E, Vozzi G, Ciardelli G, Ahluwalia A, Giusti P. Genipin-crosslinked chitosan/gelatin blends for biomedical applications. J Mater Sci – Mater Med. 2008; 19(2):889–898. [PubMed: 17665102]

37. Gorczyca G, Tylingo R, Szweda P, Augustin E, Sadowska M, Milewski S. Preparation and characterization of genipin cross-linked porous chitosan–collagen–gelatin scaffolds using chitosan–CO2 solution. Carbohydr Polym. 2014; 102:901–911. [PubMed: 24507362]
38. Lin CL, Lin CH, Chang HC, Su MC. Protein attachment on nanodiamonds. J Phys Chem A. 2015; 119(28):7704–7711. [PubMed: 25815400]
39. Suliman S, Sun Y, Pedersen TO, Xue Y, Nickel J, Waag T, Finne-Wistrand A, Steinmuller-Nethl D, Krueger A, Costea DE, Mustafa K. In vivo host response and degradation of copolymer scaffolds functionalized with nanodiamonds and bone morphogenetic protein 2. Adv Healthcare Mater. 2016; 5(6):730–742.
40. Suliman S, Xing Z, Wu X, Xue Y, Pedersen TO, Sun Y, Doskeland AP, Nickel J, Waag T, Lygre H, Finne-Wistrand A, Steinmuller-Nethl D, Krueger A, Mustafa K. Release and bioactivity of bone morphogenetic protein-2 are affected by scaffold binding techniques in vitro and in vivo. J Controlled Release. 2015; 197:148–157.
41. Zhang Q, Mochalin VN, Neitzel I, Hazeli K, Niu J, Kontsos A, Zhou JG, Lelkes PI, Gogotsi Y. Mechanical properties and biomineralization of multifunctional nanodiamond-PLLA composites for bone tissue engineering. Biomaterials. 2012; 33(20):5067–5075. [PubMed: 22494891]
42. Zhang X, Hu W, Li J, Tao L, Wei Y. A comparative study of cellular uptake and cytotoxicity of multi-walled carbon nanotubes, graphene oxide, and nanodiamond. Toxicol Res. 2012; 1(1):62–68.
43. Moore L, Yang J, Lan TTH, Osawa E, Lee DK, Johnson WD, Xi J, Chow EKH, Ho D. Biocompatibility assessment of detonation nanodiamond in nonhuman primates and rats using histological, hematologic, and urine analysis. ACS Nano. 2016; 10(8):7385–7400. [PubMed: 27439019]
44. Tsai LW, Lin YC, Perevedentseva E, Lugovtsov A, Priezzhev A, Cheng CL. Nanodiamonds for medical applications: interaction with blood in vitro and in vivo. Int J Mol Sci. 2016; 17(7):1111.
45. Solarska K, Gajewska A, Bartosz G, Mitura K. Induction of apoptosis in human endothelial cells by nanodiamond particles. J Nanosci Nanotechnol. 2012; 12(6):5117–5121. [PubMed: 22905588]
46. Eppler SM, Combs DL, Henry TD, Lopez JJ, Ellis SG, Yi JH, Annex BH, McCluskey ER, Zioncheck TF. A target-mediated model to describe the pharmacokinetics and hemodynamic effects of recombinant human vascular endothelial growth factor in humans. Clin Pharmacol Ther. 2002; 72(1):20–32. [PubMed: 12152001]
47. Moore L, Gatica M, Kim H, Osawa E, Ho D. Multi-protein delivery by nanodiamonds promotes bone formation. J Dent Res. 2013; 92(11):976–981. [PubMed: 24045646]
48. Fairbrother WJ, Champe MA, Christinger HW, Keyt BA, Starovasnik MA. Solution structure of the heparin-binding domain of vascular endothelial growth factor. Structure. 1998; 6(5):637–648. [PubMed: 9634701]
49. Suliman S, Xing Z, Wu X, Xue Y, Pedersen TO, Sun Y, Døskeland AP, Nickel J, Waag T, Lygre H, Finne-Wistrand A, Steinmüller-Nethl D, Krueger A, Mustafa K. Release and bioactivity of bone morphogenetic protein-2 are affected by scaffold binding techniques in vitro and in vivo. J Control Release. 2015; 197:148–157. [PubMed: 25445698]
50. Schimke MM, Stigler R, Wu X, Waag T, Buschmann P, Kern J, Untergasser G, Rasse M, Steinmuller-Nethl D, Krueger A, Lepperdinger G. Biofunctionalization of scaffold material with nano-scaled diamond particles physisorbed with angiogenic factors enhances vessel growth after implantation. Nanomedicine. 2016; 12(3):823–833. [PubMed: 26654993]
51. Steed DL. The role of growth factors in wound healing. Surg Clin North Am. 1997; 77(3):575–586. [PubMed: 9194881]
52. Tamama K, Kerpedjieva SS. Acceleration of wound healing by multiple growth factors and cytokines secreted from multipotential stromal cells/mesenchymal stem cells. Adv Wound Care. 2012; 1(4):177–182.

Appendix A. Supplementary data

Supplementary data associated with this article can be found, in the online version, at http://dx.doi.org/10.1016/j.actbio.2017.05.026.

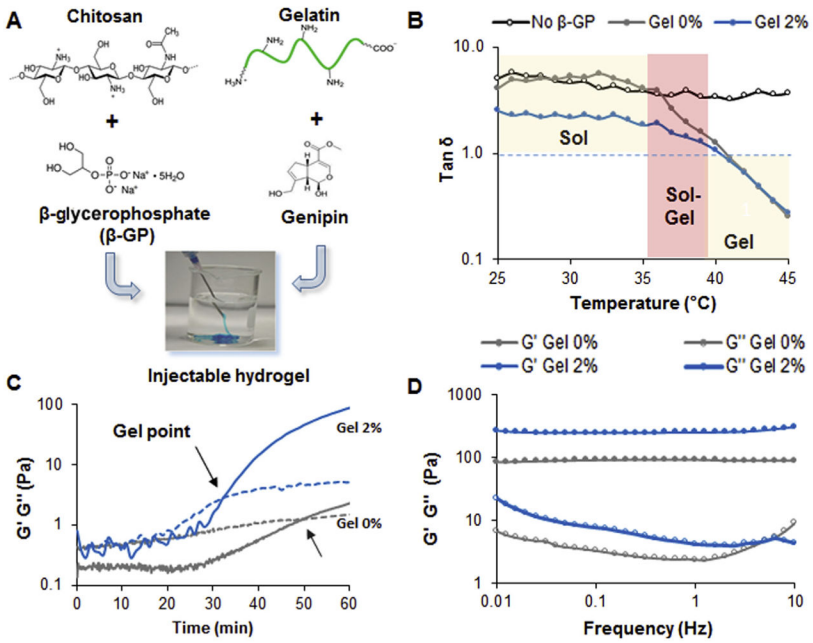

Fig. 1.

Optimization of injectable hydrogel formation A) Schematic representing the main components of the injectable hydrogels. The designed carrier is made of chitosan and gelatin using β-GP and genipin as crosslinkers. B) Temperature sweep graphs displaying the sol gel transition and the tan δ values (G″/G′) for the different systems. The group indicated as No β-GP is representative of a solution of chitosan 1.5% w/v without any β-GP. The Gel 0% and Gel 2% are systems made of chitosan at the same concentration containing β-GP and different concentration of gelatin. Genipin was kept constant at 0.02% w/v in all the groups. C) Time sweep graphs carried out at 37 °C comparing a chitosan solution 1.5% w/v without gelatin (Gel 0%) and the one with gelatin at 2% w/v (Gel 2%). The arrows indicate the cross over between G′ and G″ representative of the gel point. D) Representative frequency sweeps graphs carried out at 37 °C on the gels 24 h after their formation.

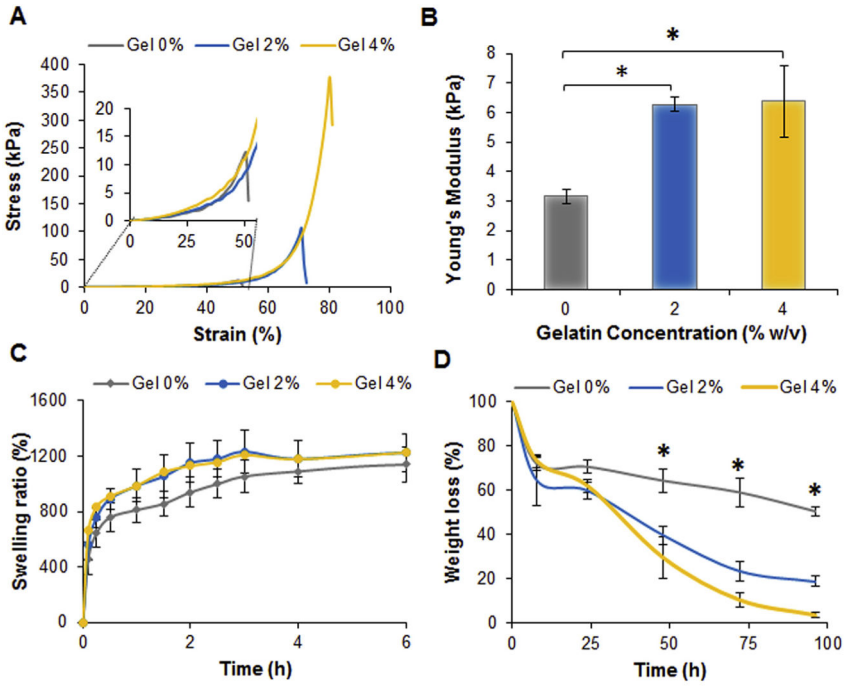

Fig. 2.

Effect of gelatin on the hydrogel mechanical and physical properties. A) Representative stress strain curves obtained compressing the fabricated hydrogels after 24 h their preparation. The insert displays the initial part of the graph to show the extreme fragility of hydrogel made only of chitosan (Gel 0%) which failed at strain lower than 50%. B) Young's Modulus values calculated from the slope of the stress strain curves at 10% of strain. Values are reported as the mean ± dev st (n = 5). * = $p < 0.05$. C) Swelling equilibrium curves of the different systems in phosphate buffer pH 7.4. Hydrogels were able to reach an equilibrium of swelling after 6 h in contact with the buffer. Results are reported as the mean ± dev st (n = 5). D) Degradation profiles of the different systems in collagenase 0.5 U/mL at 37 °C. Results are reported as the mean ± dev. st. (n = 5) * = $p < 0.05$.

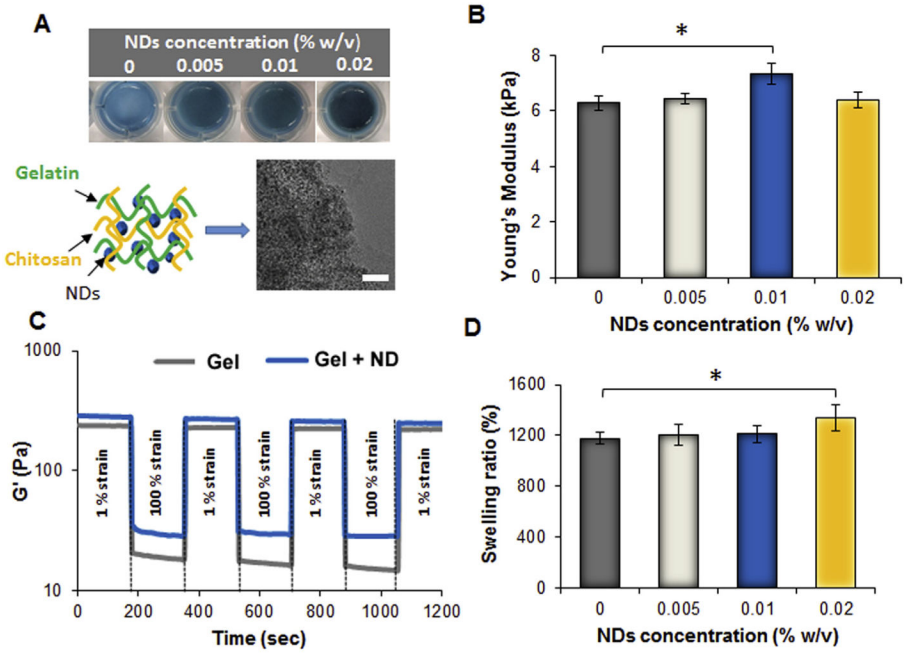

Fig. 3.

Effect of NDs on the physical and mechanical properties. A) Pictures of the injectable nanocomposite hydrogels formed in a 24 well plate and having different concentration of NDs. On the bottom, schematic representing the nanocomposite hydrogel and corresponding TEM picture of the polymeric mixture containing NDs at the concentration of 0.02% w/v prior gelation. Scale bar = 50 nm. B) Compressive Young's Modulus of the nanocomposite hydrogels containing different amount of NDs. The results are reported as mean ± dev.st (n = 5) * = $p < 0.05$. C) Representative strain cycles profiles showing the storage modulus G′ in function of time. Both the injectable hydrogel without NDs (Gel) and the group having NDs at 0.01% w/v (Gel + ND) were able to recover more than 95% of their original value. D) Swelling values obtained after soaking the hydrogel in phosphate buffer for 24 h. The results are reported as mean ± dev.st (n = 5) * = $p < 0.05$.

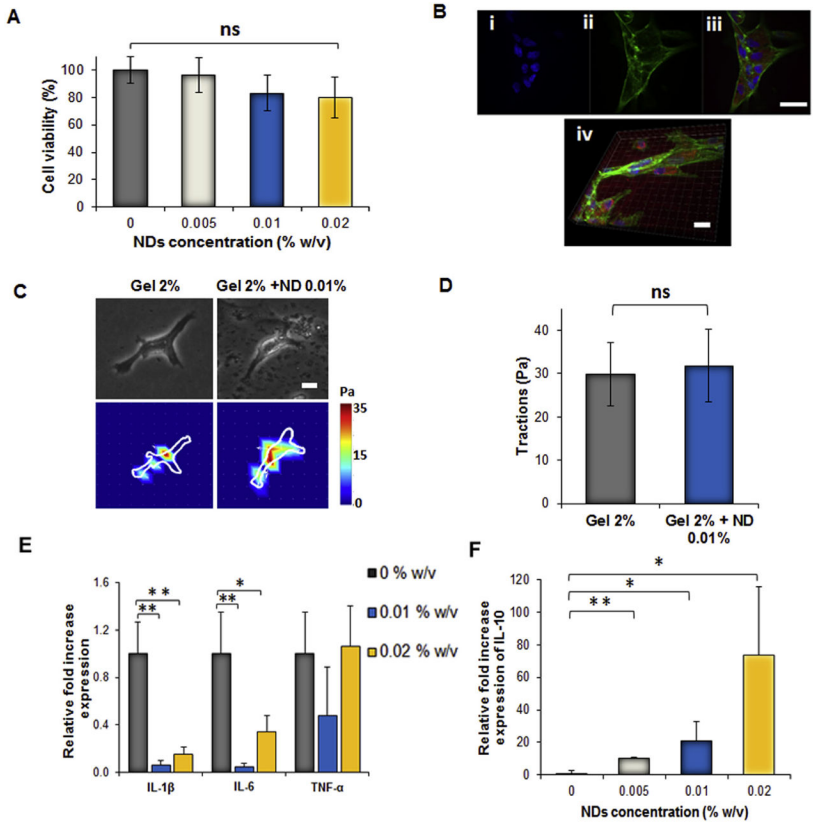

Fig. 4.

Biocompatibility studies of the nanocomposite hydrogels. A) MTS assay at 48 h on HUVECs seeded in 2D on the different nanocomposite hydrogels. No significant reduction in cell viability was observed irrespective of the concentration of NDs. B) Representative fluorescent pictures of HUVECs spreading at 48 h on the nanocomposite consisting of 0.02% w/v of NDs. The red fluorescence of the gel is mainly due to the presence of genipin. HUVECs were stained with i) DAPI to visualize the nuclei (blue), ii) with Phalloidin-Alexa Fluor 488 to stain actin (green) and iii) Mito tracker to visualize mitochondria (red). Scale bar = 20 μm. iv) Representative confocal picture of HUVECs spreading on the nanocomposite gel. Scale bar = 20 μm. C) Phase contrast pictures (scale bar = 200 μm) and traction map images of HUVECs cultured on hydrogels without NDs (Gel 2%) and nanocomposite hydrogels (Gel 2% + ND 0.01%) after 24 h. D) Root-mean-square (RMS) traction values of HUVECs indicating no increase in cell traction on the substrate containing NDs 0.01% w/v. E) Relative gene expression of the Tumor necrosis factor-α (TNF-α), Interlukin-1β (IL1-β), Interlukin-6 (IL-6) and F) the antiinflammatory Interlukin-10 (IL10) in macrophages seeded for 24 h on the nanocomposite hydrogels. Results are shown as mean ± dev. st. (n = 3) * = $p < 0.05$, ** = $p < 0.01$. (For interpretation of the references to colour in this figure legend, the reader is referred to the web version of this article.)

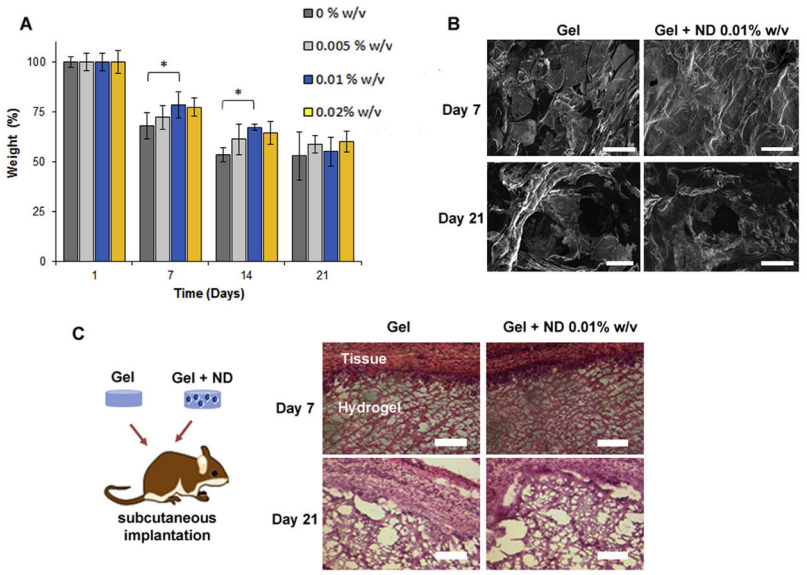

Fig. 5.

Biodegradability and biocompatibility of the nanocomposite hydrogels A) Degradation study of the nanocomposite hydrogels in PBS (pH 7.4) for 21 days. The inclusion of NDs improved the stability of the hydrogels. No significant difference was found among the groups at 21 days. Results are shown as the mean ± dev. st. (n = 5) * = $p < 0.05$. B) SEM images of the surface of the injectable hydrogels showing the degradation after 21 days. Scale bars = 300 μm C) Hydrogels with and without NDs at the concentration of 0.01% w/v were subcutaneously implanted in an immunocompetent rat model, and the gels were collected at day 7 and day 21 (n = 3). Histological analysis with H&E staining revealed no infiltration of inflammatory cells from the surrounding tissue into the hydrogel structure.

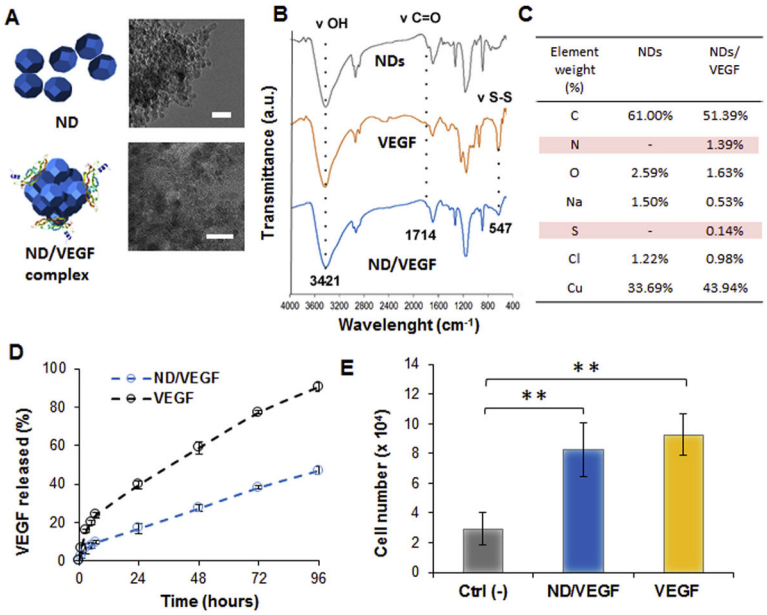

Fig. 6.

Characterization of the ND/VEGF complex and release from the nanocomposite hydrogel. A) Schematic representing ND and the complex ND/VEGF showing the protein adsorbed on the surface. On the right side corresponding TEM images of ND only and the NDs complexed with VEGF. In both images scale bar = 20 nm. B) FT-IR spectra of NDs, VEGF and the complex. C) EDX analysis of NDs with and without VEGF indicating the presence of nitrogen and sulfur in the complex. D) Release profiles from the hydrogel of VEGF alone or as complex with NDs. E) Quantification of HUVECs proliferation after 48 h. The Ctrl (-) and VEGF groups are referring to cells cultured without any growth factor or in complete supplemented media respectively. In the ND/VEGF group cells were culture in media without growth factors and treated with VEGF released from the nanocomposite hydrogels. Results are reported as the mean ± dev.st. (n = 5). ** = $p < 0.01$.

Table 1

Regressed parameters for the Korsmeyer-Peppas model.

Group	k	n	R^2
VEGF	0.094	0.473	0.998
ND-VEGF	0.032	0.571	0.997